The seventeenth International Symposium on Transport Phenomena,
4-8 September, 2006, Toyama, JAPAN

2 - D - Ⅱ - 4

THE STRUCTURE OF A BLUFF-BODY HELD FLAME CONTROLLED BY ARRAYED MICRO ACTUATORS

Y. Saiki[1], Y. Suzuki[1] and N. Kasagi[1]

[1]Department of Mechanical Engineering, The University of Tokyo, Tokyo 113-8656, Japan

ABSTRACT

An actively-controlled bluff-body held flame downstream of a coaxial nozzle is studied. Miniature flap actuators are employed to introduce disturbances locally into the initial jet shear layer. By changing the flapping frequency, the flame stability and CO emission are improved significantly. To investigate the flame structure, OH-PLIF and newly-developed conditional OH two-line methods are employed. Emission characteristics of CO and NO_x for the controlled flames are discussed on the basis of local fuel and OH radical distributions and flame temperature.

INTRODUCTION

Small-scale distributed generation (DG) systems are expected to play a major role in the future society with lower environmental impacts. Micro gas turbines (MGT) of 1-100 kW power output are considered as a core technology in the DG systems [1]. However, downsizing of such gas turbines may cause various problems. For instance, small combustors for MGT are operated at a wide range of partial load, where it is difficult to keep high combustion efficiency, low nitrogen oxides (NO_x) emission and flame stability. Since the performance of passive devices such as swirliers or flame holders is deteriorated under off-design conditions, active combustion control technology should be developed to establish ideal flame under variable load conditions.

Recently, advanced control schemes of thermal and fluid phenomena have been intensively studied. In particular, development of micro electro-mechanical systems (MEMS) has made it possible to fabricate small enough devices such as micro actuators, with which shear flow can be effectively controlled by directly introducing small disturbances into the shear layer [2].

Suzuki et al. [3] developed a miniature magnetic flap actuator, and arranged eighteen flaps on the inner wall of an axisymmetric nozzle. They created a furcating jet by modulating the phase of each flap's motion. Kurimoto et al. [4] applied the flap actuators to an axisymmetric coaxial nozzle. They installed the flaps on the inner surface of the annular nozzle and manipulated the near-field vortical structures in a coaxial jet. They could flexibly control methane/air mixing by changing the flapping frequency.

The objectives of the present study are to apply the coaxial nozzle [4] to a bluff-body held flame for improving the CO/NO_x emission and the stability, and to investigate the mechanism responsible for the flame characteristics with the aid of PLIF techniques. Mixture fraction of fuel was investigated through acetone-PLIF method. To assess the combustion reaction, an OH-PLIF method was employed. In addition, a conditional OH two-line method has been developed to measure temperature distributions by using one-set laser and detection system.

EXPERIMENTAL SETUP

Flow facility

Figure 1 shows a coaxial nozzle equipped with miniature magnetic flap actuators on the inner surface of the annular nozzle. The flap is made of a copper-plated polyimide film of 9 mm in length and 3 mm in width. The thicknesses of polyimide and copper layers are 25 μm and 35 μm respectively. A single-turn coil is patterned on the copper layer using photolithography [3]. When an electrical current is applied to the copper coil, the flap is elastically bent by the magnetic force between the coil and a cylindrical permanent magnet embedded in the nozzle wall.

An dry air jet at room temperature was supplied vertically into a combustion chamber with 200 mm height and 40 × 40 $(mm)^2$ square cross section through an annular nozzle (inner diameter D_i = 10 mm, outer diameter D_o = 20 mm). A central methane jet was supplied from a long straight tube, in which a fully-developed laminar flow was established. The bulk mean velocities of central and annular jets were set to be $U_{m,i}$ = 0.38 m/s and $U_{m,o}$ = 1.8 m/s. The Reynolds number of the annular jet, $U_{m,o}D_o/\nu_o$, and the momentum flux ratio, $\rho_o U_{m,o}^2/\rho_i U_{m,i}^2$, are 2.4×10^3 and 42, respectively. Hereafter, z and r denote the streamwise and radial directions, respectively.

A flame was held with a ring type bluff-body (inner diameter 8 mm, outer diameter 12.75 mm, thickness 0.95 mm), or was located at z/D_o = 1.5. The flame was operated at an overall fuel-to-air equivalence ratio of ϕ = 0.72 and a thermal power of 1.1 kW.

In this study, the motion of the flap actuators are all synchronized. The voltage signal for flapping motion was a saw-wave form, which is the most effective for mixing [4]. After reaching the maximum displacement of 0.3 mm, the flaps snap quickly back to the wall. The Strouhal number St_a (= $f_a D_o/U_{m,o}$) is defined with the flapping frequency f_a, and St_a was changed from 0.1 to 2.5.

Measurement system

Schematic of the measurement system is shown in Fig. 2. Flame characteristics were evaluated by the CO/NO_x

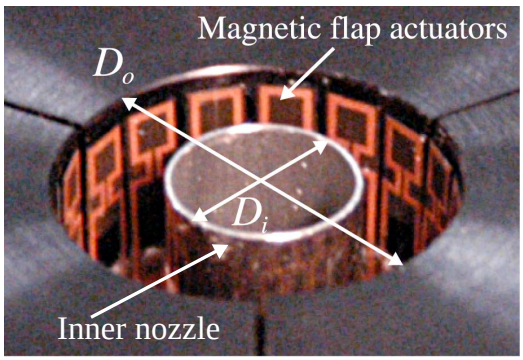

Fig. 1. Coaxial nozzle equipped with eighteen miniature magnetic flap actuators.

emission and the heat release fluctuations. The exhaust gas was sampled by a stainless tube at z/D_o = 20, where chemical reaction was considered to be frozen. The sampled gas was analyzed by an exhaust gas analyzer (Horiba, MEXA-4000FT). The amount of emissions is evaluated as volumetric fractions at 15% O_2. The CH radical chemiluminescence, which corresponds to the heat release fluctuations, was measured by a photomultiplier (Hamamatsu, R329-02) equipped with an interference filter centered at 431.4 nm.

For the measurement of acetone and OH fluorescence, UV laser light pulse was generated with a frequency-doubled dye laser (Lambda Physik, SCANmate2C), which is pumped by a frequency-doubled Nd: YAG laser (Quantel, LPY400). The laser beam was formed into a laser sheet of constant height (50 mm) and thickness (0.5 mm) by using cylindrical and spherical lenses. The laser sheet was introduced into the test section through a quartz window of the combustion chamber.

In the acetone-PLIF measurement, 283.0 nm UV light was chosen. To investigate the mixture fraction, the inner methane flow was seeded with acetone vapor by bubbling the career gas into a liquid acetone container [5]. In the OH-PLIF measurement, the spectral line $Q_1(8)$ (283.553 nm) of $A^2\Sigma^+ \leftarrow X^2\Pi(1,0)$ was excited. The fluorescence intensity taken by this transition is proportional to mole fraction of OH radical [6]. The typical pulse energy is 5 mJ/pulse and the resulting averaged energy density in the measurement plane is 20 mJ/cm^2/pulse.

The fluorescence signal was detected with an image-intensified CCD camera (La Vision, Flamestar2) of 576 × 384 pixels^2 using 105 mm UV lens (Nikon, UV Nikkor 105mm F4.5D) as well as a low-pass optical filter having a cutoff wavelength of 295 nm in order to eliminate the Mie scattering from dust particles. The gain of the image intensifier was fixed at 4.41 counts/ph.el. The field of view is 60 × 40 (mm)^2. In order to reduce the effect of shot noise, fluorescence signals in subregions of 4 × 4 pixels^2 are ensemble-averaged, and this results in a spatial resolution of 0.4 × 0.4 (mm)^2.

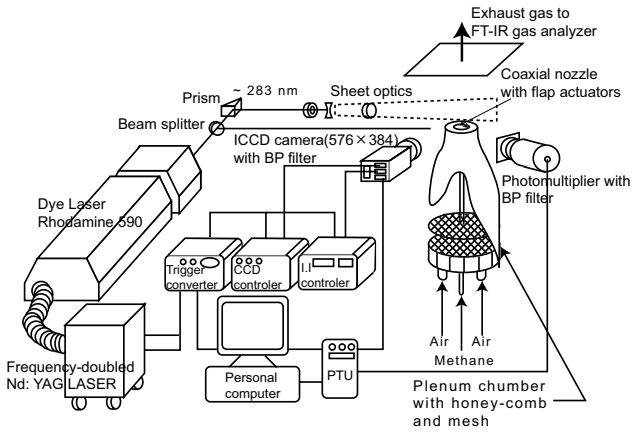

Fig. 2. Schematic of measurement system.

CONDITIONAL OH TWO-LINE METHOD

Laser-based techniques are frequently used to assess concentration and temperature fields noninvasively. To investigate turbulent flame structures, planar laser-Induced fluorescence (PLIF) of OH radicals are commonly used. Since OH radicals exist widely and abundantly in burned gas, OH-PLIF measurement is useful to visualize and assess a combustion reaction field. In addition, PLIF methods can be used to deduce flame temperature distribution from the relative populations of two rotational states of an atomic or molecular species [7-12]. In an OH two-line PLIF method, the flame temperature T can be calculated from the OH fluorescence intensity ratio detected by exciting two different rotational states I_1/I_2, i.e.,

$$T = \frac{\Delta E}{k}\left[\ln\left(\frac{I_1}{I_2}\right)\cdot\frac{E_2}{E_1}\cdot\frac{B_2}{B_1}\cdot\frac{2J_2''+1}{2J_1''+1}\right]^{-1}, \quad (1)$$

where ΔE, k, E, B and J'' are the quantum energy difference between two rotational levels, the boltzmann constant, the laser intensity, the Einstein coefficient for absorption, and the rotational quantum number respectively. Subscripts 1 and 2 denote different rotational levels in the ground state.

When a single excitation laser and a single detection camera are employed, temperature measurement based on Eq. (1) can be applied only to steady laminar flames. In the present study, a conditional OH two-line method has been developed in order to measure temperature field of unsteady flame. In this method, ensemble-averaged OH fluorescence intensities at the flame front, which are taken by two excited lines, are used. First, the flame front was extracted from instantaneous OH-PLIF images with two different excitation lines by tracing the maximum OH concentration at each streamwise distance as shown in Fig. 3. Then, ensemble-averaged I_1/I_2 at each streamwise position is estimated and one-dimensional flame temperature distribution is calculated by Eq. (1).

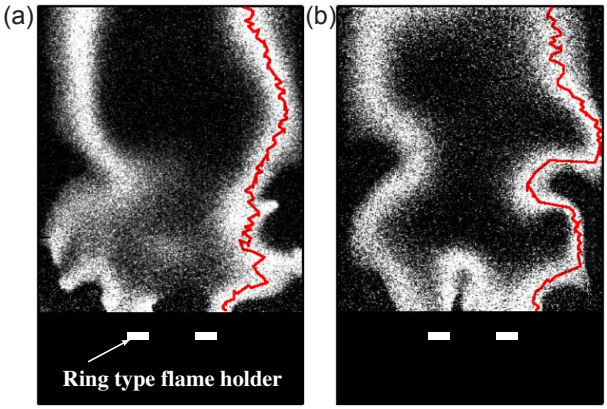

Fig. 3. Instantaneous OH-PLIF images. (a) and (b) are excited at different transitions. Bold lines denote flame front.

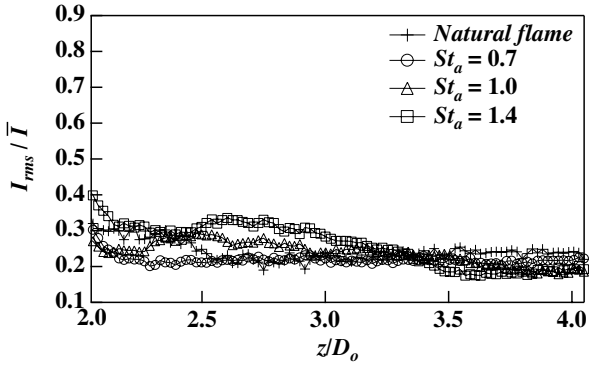

Fig. 4. RMS value of OH concentration at flame front.

Figure 4 shows the root-mean-square value of OH concentration fluctuation at the flame front for the $Q_1(8)$ transition. The fluctuation of OH concentration is around 30 percent of the mean concentration in all flames.

Hanson et al. [8] suggested candidates of excitation lines for OH two-line thermometry. They show that the measurement accuracy can be improved by fitting $\Delta E/k$ in Eq. (1) with the peak temperature in the flame. Since the maximum temperature of the present flame is estimated at around 2000 K, $R_2(5)$ and $Q_1(10)$ or $P_1(7)$ and $Q_2(11)$ transitions should be preferable.

In the conditional OH two-line method, the location of the maximum OH concentration should coincide with that of the maximum fluorescence. Therefore, the excitation lines which are less thermally dependent must be selected. Figure 5 shows the thermal dependence of each tansition, where $f(T)$ is the boltzmann function. We employ the combination of $P_1(7)$ and $Q_2(11)$ transitions because of its lower thermal dependence,

Mean pulse energy densities of the two lines were about 8mJ/cm²/pulse, which is sufficiently low to avoid saturation and to minimize the influence of the different rotational energy transfer rates in the ground state [13].

The uncertainly of the conditional OH two-line method was systematically investigated. The elemental errors are the shot noise, the pulse jitter of the laser center wavelength, and the fluctuation of the OH concentration. As a result, the uncertainly interval estimated at 95% coverage is 135.6 K for the mean temperature of 2000 K.

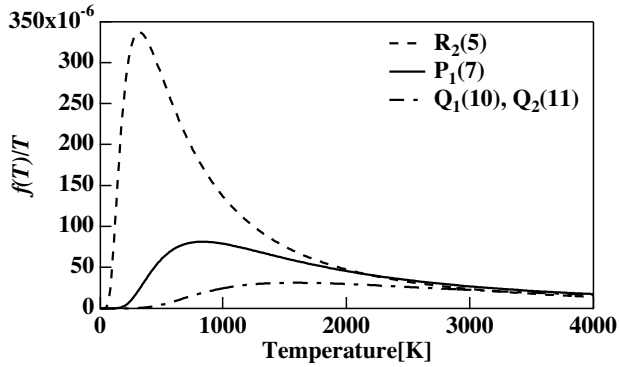

Fig.5. Thermal dependence of excitation lines for OH two-line method.

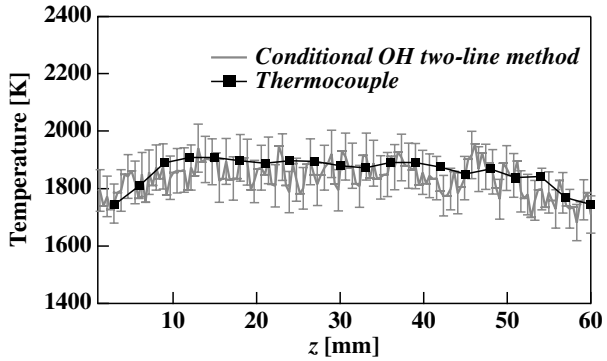

Fig.6. Mean flame temperature distribution in laminar flame.

The measurement accuracy of the present conditional OH two-line method was evaluated for laminar flame using a Bunsen burner. Figure 6 shows the mean flame temperature distributions in the streamwise direction measured with the present method. The temperature at the flame front was also measured with a thermocouple made of 100 μm diameter 30:6 Rh-Pt wires with silica coating. These two measurements agree well within the uncertainty intervals.

RESULTS AND DISCUSSION

Flame characteristics

Characteristics of the controlled flame are shown in Table 1. The index of heat-release fluctuations i^*, which is evaluated by the CH radical chemiluminescence, is defined as:

$$i^* = \frac{\sqrt{\overline{I'^2}}/\bar{I}}{\sqrt{\overline{I_o'^2}}/\bar{I}_o}, \qquad (2)$$

where $\sqrt{\overline{I_o'^2}}/\bar{I}_o$ represents the fluctuations of the chemiluminescence in the natural flame.

Kurimoto et al. [10] shows that the mixing of methane/air coaxial jet is most enhanced at St_a = 1.0. Under this condition, i^* and the emission of CO are reduced. When St_a = 0.7, the CO emission can be reduced by up to 50

Table 1. Characteristics of bluff-body held flame.

	*i**	CO [ppm at 15%O_2]	NO_x [ppm at 15%O_2]
Natural	1	151 ± 5.8	23 ± 8.5
St_a = 0.7	0.74	71 ± 4.1	22 ± 6.1
St_a = 1.0	0.77	87 ± 4.1	22 ± 6.1
St_a = 1.4	0.53	95 ± 3.5	22 ± 5.2

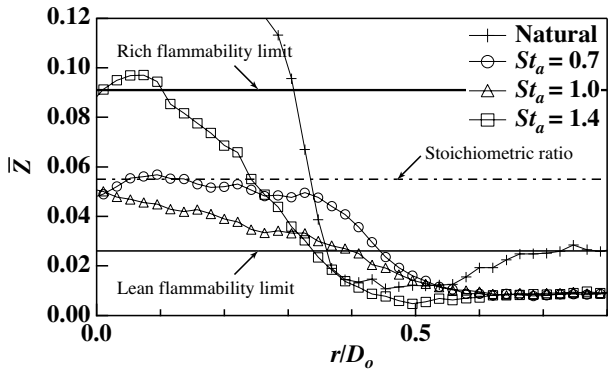

Fig. 7. Radial distribution of mean mixture fraction of methane at z/D_o = 1.4.

percent of the natural flame. At St_a = 1.4, the heat release fluctuation is most suppressed. On the other hand, the NO_x emission is unchanged in all flames. In the following section, the mechanisms responsible for the observed flame characteristics are discussed.

Mixture fraction measurement in cold jet

To estimate the distribution of fuel concentration, acetone-PLIF measurement is employed in cold jets. Figure 7 shows the radial distribution of ensemble-mean mixture fraction of methane in the upstream region of the flame holder which is located at z/D_o = 1.4. The mixture fraction is calculated from the acetone fluorescence intensities. The rich/lean flammability limit and the stoichiometric ratio are also shown. In the controlled jets, mixing of methane/air is enhanced by intense vortex shedding [4]. When St_a = 1.0, mixing is most enhanced by large-scale vortices [4], and thus fuel-lean mixture is supplied to the flame. On the other hand, when St_a = 1.4, local mixing is achieved by small-scale vortices [4], and thus mixture which is close to rich flammable limit is supplied locally.

OH-PLIF measurement

Figure 8 shows raw images of the bluff-body held flame. In the natural flame, the total flame length is approximately $9D_o$ and a luminous light emission is frequently observed, and this fact implies slow and incomplete combustion. In the controlled flame, or especially when St_a = 1.0, the total flame length is markedly reduced to about $6D_o$, and blue chemiluminescent emission is observed. Therefore, with the present control, rapid and relatively complete combustion is achieved in the flame.

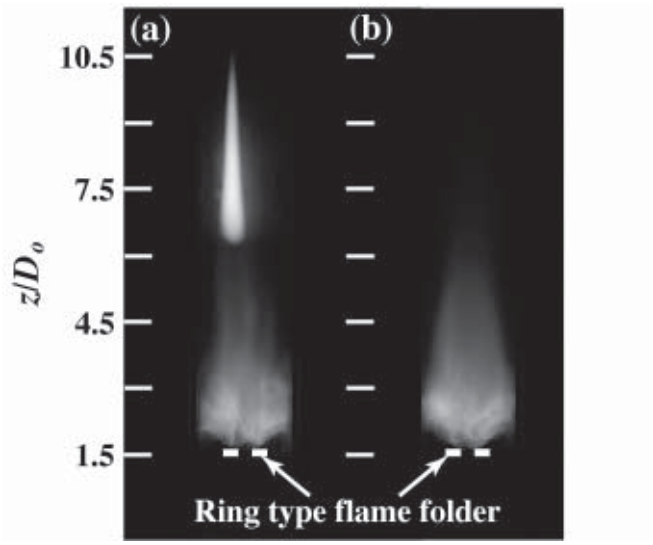

Fig. 8. Raw images of bluff-body held flame.
(a) Natural flame and (b) Controlled flame for St_a = 1.0.

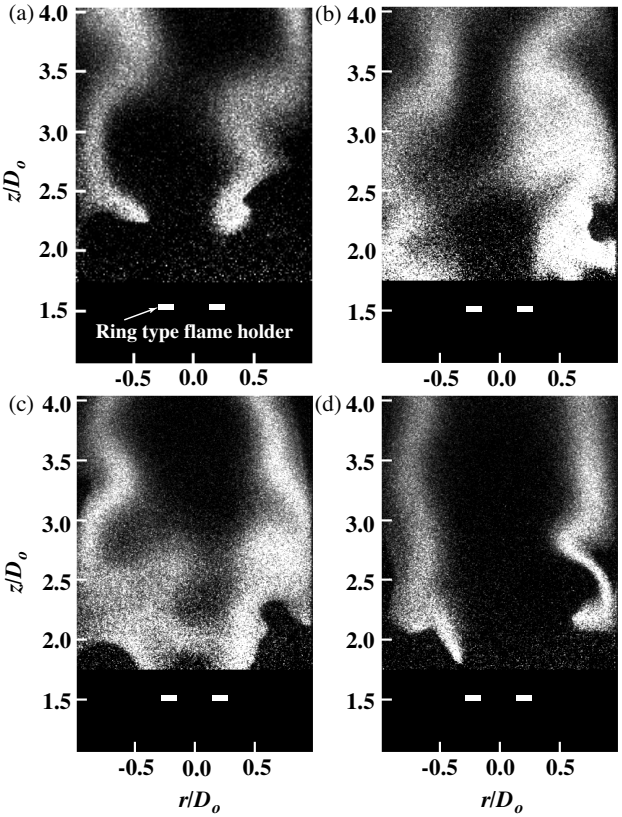

Fig. 9. Snap shots of OH-PLIF images:
(a) Natural flame, (b) St_a = 0.7, (c) St_a = 1.0 and (d) St_a = 1.4.

Figure 9 shows typical instantaneous OH-PLIF images of the natural and the controlled flames in the central longitudinal plane. OH distributions are wrinkled by the effect of turbulence. In the natural flame, quenching of the chemical reaction is often observed near the flame base (z/D_o < 2.0). On the other hand, when St_a = 0.7 and 1.0, OH radicals are widely distributed, so that it is anticipated that the burning rate is much increased. It is because mixing upstream is enhanced under these condi-

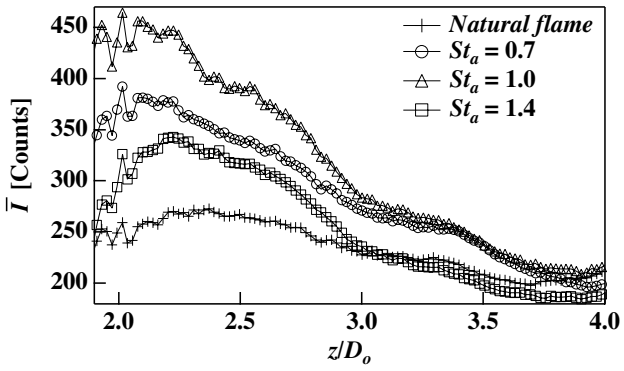

Fig. 10. Streamwise mean OH distribution at flame front.

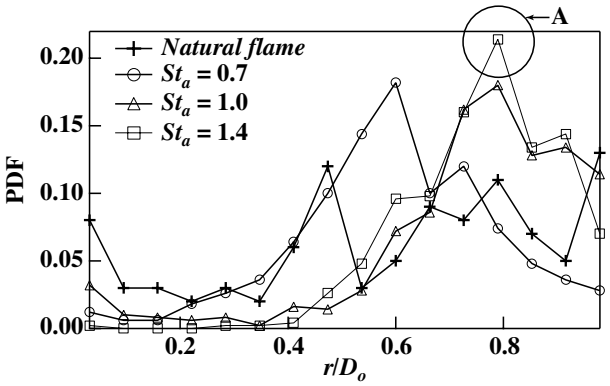

Fig. 11. PDF of radial flame front position at z/D_o = 3.0.

tions and flammable mixture is supplied to the flame as shown in Fig. 7.

In order to evaluate the intensity and stability of combustion reaction quantitatively, the flame front was extracted from the instantaneous OH images as shown in Fig. 3. Figure 10 shows the streamwise distribution of ensemble-mean OH intensity at the flame front. OH intensities of the controlled flames are increased when compared to that of the natural flame. In particular, when St_a = 0.7 and 1.0, the OH intensities at the flame base becomes 1.5 ~ 2.0 times larger. Since the mixing is enhanced and highly oxygenated mixture is supplied to the flame, the OH intensity is maximized at St_a = 1.0.

On the other hand, OH radical plays an important role as an oxidizer in CO oxidizing reaction. Therefore, CO emission reduction is partially due to the fact that OH radical is distributed widely in these controlled flames and its concentration is increased.

Figure 11 shows the probability density function (PDF) of radial flame front position at z/D_o = 3.0. In the natural flame, the flame front is fluctuated widely in the radial direction. On the other hand, in the controlled flame, the fluctuation of flame fronts is suppressed and the PDFs have a peak at r/D_o > 0.6. Particularly, when St_a = 1.4, the fluctuation is most suppressed . (A in Fig. 11). The stabilization of the flame front implies that velocity fluctuations in the combustion field become small, and consequently the ignition and propagation of the flame are

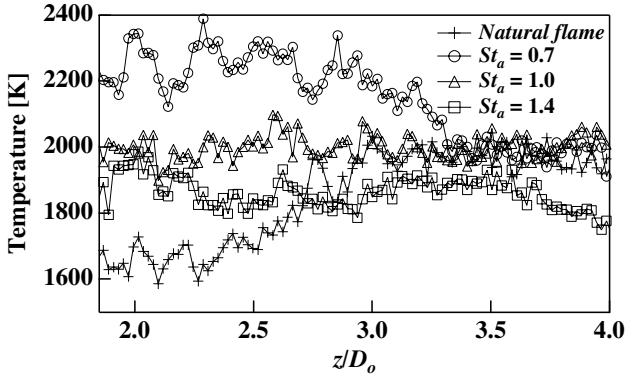

Fig. 12. Streamwise mean flame temperature distribution.

not disturbed. This is in accordance with the fact that the heat release fluctuation is most suppressed at St_a = 1.4.

Flame temperature measured with conditional OH two-line method

Figure 12 shows the streamwise mean temperature distributions of the natural and the controlled flames, which are measured with the conditional OH two-line method. Each data point represents an ensemble-average over 250 instantaneous fields. In the natural flame, the mean temperature at z/D_o ~2.0 is relatively low (~ 1650 K) due to quenching of chemical reaction around the flame base. Note that, because OH is not always present when quenching occurs, the mean temperature distribution where quenching occurs can be biased. On the other hand, in the controlled flame at St_a = 0.7, the maximum mean temperature is the highest (~ 2200 K) . It is because vortex shedding is intermittent at St_a = 0.7, and the mixture with stoichiometric plane is supplied to the flame as shown in Fig. 6. Since CO oxidizing reaction strongly depends on the mean flame temperature, CO emission is drastically reduced for St_a = 0.7.

The formation of NO_x is known to be dominated by prompt and thermal NO_x mechanisms. Prompt NO_x rate depends on fuel concentration of mixture, while thermal NO_x rate depends on flame temperature and residence time of combustion gas. From the aspect of the maximum mean flame temperature, thermal NO_x is produced in all flames. In the controlled flame for St_a = 1.4, the mean flame temperature is approximately 1850 K, which is considerably lower than that at St_a = 0.7, and thus thermal NO_x is reduced. On the other hand, fuel-rich mixture is supplied to the flame as shown in Fig. 7. Therefore, it is contemplated that the prompt NO_x production is increased in this controlled flame. Although the temperature is quite low at flame base in the natural flame, the flame length becomes long as shown in Fig. 8. It means that the residence time of combustion gas becomes long, so that the thermal NO_x formation is increased downstream of the flame. These are the primary reasons for the NO_x emission, which is approximately constant in all flames.

CONCLUSIONS

The structure of an actively controlled bluff-body held flame with arrayed miniature magnetic flap actuators was studied. In order to investigate the mechanism responsible for the flame characteristics, OH-PLIF and newly developed conditional OH two-line methods were employed. The following conclusions can be derived:

1. The CO emission and the heat release fluctuation are improved by manipulating methane/air mixing with the flap actuators.
2. The streamwise mean temperature distribution of a bluff-body held flame was measured with an uncertainty interval of 135.6 K at 2000 K by the conditional OH two-line method.
3. When St_a equals 0.7, the combustion reaction occurs in a highly-oxygenated and high temperature field, so that the CO emission is drastically reduced.
4. When St_a equals 1.4, the fluctuation of flame front is most suppressed, and this causes reduction in the heat release fluctuations.
5. Because of the balance of local fuel concentration, mean flame temperature and residence time, the NO_x emission remains approximately constant in all flames.

ACKNOWLEDGMENTS

The authors deeply thank Dr. N. Kurimoto for variable discussion during the course of this work. The present work was supported through the 21st Century COE Program, “Mechanical Systems Innovation,” by the Ministry of Education, Culture, Sports, Science and Technology.

NOMENCLATURE

B Einstein coefficient for absorption, dimensionless
D_i inner nozzle diameter of the coaxial nozzle, mm
D_o outer nozzle diameter of the coaxial nozzle, mm
ΔE quantum energy difference, J
E laser energy intensity, mJ/pulse
$f(T)$ Boltzmann function, dimensionless
f_a flapping frequency, Hz
I OH fluorescence intensity, counts
i^* heat release fluctuation index, dimensionless
J'' rotational quantum number, dimensionless
k Boltzmann constant, J/K
r radial distance from the center of the nozzle, mm
St_a Strouhal number (= $f_a D_o / U_o$), dimensionless
T flame temperature, K
$U_{m,o}$ bulk mean velocity of the annular jet, m/s
$U_{m,i}$ bulk mean velocity of the inner jet, m/s
z streamwise distance from the exit of the nozzle, mm
Z mixture fraction of methane, dimensionless
ϕ equivalence ratio, dimensionless
ν_o kinematic viscosity coefficient of air, m^2/s
ρ_i density of methane, kg/m^3
ρ_o density of air, kg/m^3

REFERENCES

1. Kimijima S, Kasagi N, Cycle analysis of micro gas turbine-molten carbonate fuel cell hybrid system, Int JSME J, B, 48, 65-73 (2005).
2. Ho CM, Tai YC, Review: MEMS and its applications for flow control, ASME Int Fluids Eng, 118, 437-447 (1996).
3. Suzuki H, Kasagi N, Suzuki Y, Active control of an axisymmetric jet with distributed electromagnetic flap actuators, Exp in Fluids, 36, 498-509 (2004).
4. Kurimoto N, Suzuki Y, Kasagi N, Active control of coaxial jet mixing with arrayed micro actuators, JSME J B (in Japanese), 70, 1417-1424 (2004).
5. Lozano A, Yip B, Hanson R.K, Acetone: a tracer for concentration measurements in gaseous flows by planar laser-induced fluorescence, Exp Fluids, 13, 369-376 (1992).
6. Allen M.G, Parker T.E, Reinecke W.G, Legner H.H, Foutter R.R, Rawlins W.T, Davis S.J, Fluorescence imaging of OH and NO in a model supersonic combustor, AIAA J, 31, 505-512 (1993).
7. Cattolica R, OH rotational temperature from two-line laser-excited fluorescence, Applied Optics, 20, 1156-1166 (1981).
8. Seitzmann J.M, Hanson R.K, DeBarber P.A, Hess C.F, Application of quantitative two-line OH planar laser-induced fluorescence for temporally resolved planar thermometry in reacting flows, Applied Optics, 33, 4000-4012 (1994).
9. Giezendanner T.R, Meier U, Meier W, Heinze J, Aigner M, Phase-locked two-line OH planar laser-induced fluorescence thermometry in a pulsating gas turbine model combustor at atmospheric pressure, Applied Optics, 44, 6565-6577 (2005).
10. Lee M.P, Mcmillin B.K, Hanson R.K, Temperature measurements in gases by use of planar laser-induced fluorescence imaging of NO, Applied Optics, 32, 5379-5396 (1993).
11. Tamura M, Luque J, Harrington J.E, Berg P.A, Smith G.P, Jeffries J.B, Crosley D.R, Laser-induced fluorescence of seeded nitric oxide as a flame thermometer, Applied Physics B, 66, 503-510 (1998).
12. Bessler W.G, Hidenbrand F, Schulz C, Two-line laser-induced fluorescence imaging of vibrational temperatures in a NO-seeded flame, Applied Optics, 40, 748-756 (2001).
13. Daily J.W, Rothe E.W, Effect of laser intensity and of lower-state rotational energy transfer upon temperature measurements made with laser-induced fluorescence, Applied Physics B, 68, 131-140 (1999).